Organic-Inorganic doped Nickel Oxide Nanocrystals for Hole Transport Layers in Inverted Polymer Solar Cells with Color Tuning

Riva Alkarsifi, Yatzil Alejandra Avalos-Quiroz, Pavlo Perkhun, Xianjie Liu, Mats Fahlman, Anil Kumar Bharwal, Carmen M. Ruiz, David Duché, Jean-Jacques Simon, Christine Videlot-Ackermann, et al.

Organic-Inorganic doped Nickel Oxide Nanocrystals for Hole Transport Layers in Inverted Polymer Solar Cells with Color Tuning

Riva Alkarsifi[1], Yatzil Alejandra Avalos-Quiroz[1], Pavlo Perkhun[1], Xianjie Liu[2], Mats Fahlman[2], Anil Kumar Bharwal[3], Carmen M. Ruiz[3], David Duché[3], Jean-Jacques Simon[3], Christine Videlot-Ackermann[1], Olivier Margeat[1*] and Jörg Ackermann[1*]

[1] Aix Marseille Univ, CNRS, CINaM, FUN-PV group, Marseille, France.
[2] Laboratory for Organic Electronics, ITN, Linköping University, Norrköping, Sweden.

[3] Aix Marseille Univ, Université de Toulon, CNRS, IM2NP, FUN-PV group, Marseille, France.

[*] Corresponding Authors:
E-mail address: olivier.margeat@univ-amu.fr
ackermann@cinam.univ-mrs.fr

KEYWORDS:

Nickel oxide; doping; interfacial layer; morphology; hole transport; solar cell.

Abstract

Polymer solar cells using non-fullerene acceptors are nowadays amongst the most promising approaches for next generation photovoltaic applications. However, there are still remaining challenges related to large-scale fully solution-processing of high efficiency solar cells as high efficiencies are obtained only at very small areas using hole transport layers based on evaporated molybdenum oxide. Solution-processable hole transport materials compatible with non-fullerene acceptor materials are still scarce and thus considered as one of the major challenges nowadays. In this work, we present copper-doped nickel oxide nanocrystals that form highly stable inks in alcoholic-based solutions. This allows processing efficient hole transport layers in both regular and inverted device structures of polymer solar cells. As the initial work function of these ionic doped materials is too low for efficient hole extraction, doping the nanocrystals with an organic electron acceptor, namely 2,3,5,6-tetrafluoro-7,7,8,8-tetracyanoquino dimethane (F4-TCNQ) was additionally applied to make the work function more suitable for hole extraction. The resulting hybrid hole transport layers were first studied in polymer solar cells based on fullerene acceptors using regular device structures yielding in 7.4% efficiency identical to reference cells based on poly (3,4-ethylenedioxythiophene) polystyrene sulfonate (PEDOT:PSS). For inverted device structures, the hybrid hole transport layers were processed on top of blends based on the non-fullerene acceptor IT-4F and PBDB-T-2F donor. The corresponding solar cells lead promising efficiencies up to 7.9% while the reference devices using PEDOT:PSS show inferior performances. We further show that the hybrid hole transport layer can be used to tune the color of the polymer solar cells using optical spacer effects.

1. Introduction

The low cost, flexibility, light weight and solution-processability enable the polymer solar cells (PSC) technology to be used in large-scale industrial applications. The intense researches in the field of polymer photovoltaics during the last 10 years brought the power conversion efficiency (PCE) up to over 18%.[1] This high efficiency drives PSCs to be one of the most promising new generation of photovoltaic solar panels. This technological progress was made possible by developing new materials in the active layer, especially the new low band gap donor materials as well as the non-fullerene acceptors (NFAs). The presence of interfacial layers (ILs) between the photoactive layer and the electrodes is also one of the critical aspects for the fabrication of highly efficient and stable optoelectronic devices. Efficient ILs improve the charge carrier extraction toward the electrodes, avoid non ohmic contact losses as well as charge carrier recombination and exciton quenching at the interfaces.[2] Typically, an effective hole transport layer (HTL) should possess good optical transparency and efficient electron-blocking ability with suitable hole transport properties.[3] Furthermore, the conductivity should be high enough to process layers up to several hundreds of nanometers to guaranty robust printing of HTLs. Poly(3,4-ethylenedioxythiophene):poly(styrene-sulfonate) (PEDOT:PSS) with a work function (WF) of 5.10 eV has been widely used as a HTL in regular device structures.[4] It has even been used, in its highly conductive formulations, after treatments with acid[5] or polar solvents,[6] as electrode itself for ITO replacement.

Despite the high efficiencies obtained, most of the commercial PEDOT:PSS solutions have a pH value between 1 and 3 at 20 °C that causes etching of indium from ITO electrode. The indium diffusion into the photoactive layer induces fast device degradation. Thus, to overcome the acidity problem, and thereby improve device stability, Meng *et al*.[7] introduced pH neutral PEDOT:PSS as HTL in bulk heterojunction (BHJ) devices with a photoactive layer of poly[N-9″-hepta-decanyl-2,7-carbazole-alt5,5-(4′,7′-di-2-thienyl-2′,1′,3′-benzothiadiazole] (PCDTBT) and [6,6]-phenyl C71 butyric acid methyl ester ($PC_{70}BM$). Interestingly, the double treatment of the pH-neutral PEDOT:PSS surface with UV-ozone and oxygen plasma not only improves the PCE to 6.60% when compared to the acidic PEDOT:PSS-based devices (6.28%) but also enhances air stability.

However, as PEDOT:PSS is highly hydrophilic, processing inverted device structures in which PEDOT:PSS has to be solution-processed on top of the photoactive layer leads to poor film morphology and worse electrical properties.[8] Such wettability problems on hydrophobic surfaces can be solved by adding proper additives capable of reducing the hydrophilic nature of PEDOT:PSS. However, by using modified PEDOT:PSS HTLs for inverted device structures, still low efficiencies were obtained.[8,9,10] Thus, these limitations necessitate the replacement of PEDOT:PSS with other solution-processed hole transport materials,[11] especially for processing inverted device structures. Other materials stand out as promising candidates to replace PEDOT:PSS HTLs such as the well-known stable transition metal oxides (TMOs) including molybdenum oxide (MoO_3), tungsten oxide (WO_3), vanadium oxide (V_2O_5), ~~and~~ nickel oxide (NiO_x)[11,12] and ternary metal oxides.[13,14,15] Indeed for the later ones, the features of low-cost, low-temperature, simplicity, ligand-free, and solution processability expose the opportunities to be used for large-scale and flexible high performance PSCs.

Among all metal oxides, NiO_x shows advantages including good electron-blocking ability, p-type conductivity and wide band gap with high ionization potential that promotes an ohmic contact at the BHJ/anode interface.[16] Additionally, the valence band of NiO_x is well aligned with the highest occupied molecular orbital (HOMO) levels of many typical p-type conjugated polymers for hole transport which is distinct from other typical oxide-based materials.[17,18]

NiO_x HTLs have been prepared for PSCs by various processing methods, such as pulsed laser deposition,[19] sputtering,[20] thermal evaporation,[21] atomic layer deposition[22] and solution processes.[23] Among these, solution-processed methods are highly desirable as they meet the requirements for low-cost, large-scale and roll-to-roll production.

Primary, the studies on solution-processed NiO_x HTLs were focused on utilizing the sol-gel method.[24] Normally, this method requires post-treatments such as high temperature annealing or oxygen-plasma exposure to convert the deposited precursor solution into NiO_x thin films. Such treatments limit the incorporation of the prepared NiO_x in flexible and inverted device structures. Thus, an alternative colloidal nanocrystal approach is favored. The main advantage of this approach is decoupling the particle synthesis from the film-formation process with the utilization of lower temperature annealing step[18,25], allowing for their use in flexible and inverted PSCs.[26]

In this work, we focused on the solution-processed NiO_x HTLs prepared by the chemical precipitation method. So far, pristine NiO_x nanoparticles (NPs) synthesized using the chemical precipitation method were employed mostly for inverted-based perovskite solar cells.[27,28,29] The only example utilizing the chemically precipitated aqueous NiO_x solutions in PSCs was given by Jiang *et al*.[18] The HTLs were prepared by spin-coating without any post-treatments during device fabrication and resulted in PCE of 9.16% and 7.96% with PTB7-Th:$PC_{70}BM$ and PTB7:$PC_{70}BM$-based regular PSCs, respectively. Importantly, the reported NiO_x NPs were dispersed in water, thus they are not compatible for processing on top of hydrophobic photoactive layers. Recently, self-assembled quasi-3D nanocomposite of NiO_x nanocrystals and graphene oxide (GO) nano-sheets in ethanol have been developed for highly efficient and stable inverted organic solar cells based on fullerene and non-fullerene acceptors. Due to enhanced conductivity and electron blocking ability of the nanocomposite, J_{SC} and FF were both enhanced and the highest PCE obtained was 12.31% using a combination of the polymer donor named poly[(2,6-(4,8-bis(5-(2-ethylhexyl)thiophen-2-yl)benzo[1,2-b:4,5-b′]dithiophene)-co-(1,3-di(5-thiophene-2-yl)5,7-bis(2-ethylhexyl)-benzo[1,2-c:4,5-c′]dithiophene-4,8-dione)] (PBDB-T) and the non-fullerene acceptor named 3,9-bis(2-methylene-((3-(1,1-dicy anomethylene)-6/7-methyl)-indanone))-5,5,11,11-tetrakis(4-hexylphenyl)-dithieno[2,3d:2',3'-d']-s-indaceno [1,2-b:5,6-b']dithiophene (IT-M).[30] The self-assembled quasi-3D nanocomposite could also break the conductivity limitation of the 2D-GO material, as up to 32 nm thick HTLs could be included in the device without generation of any important performance loss. To further increase layer thickness and thus processing robustness of HTLs for industrial printing processes, the increase of electrical conductivity of NiO_x, via metal ion doping is an effective approach. Jung *et al*.[31] demonstrated a Cu-doped NiO_x HTL prepared via combustion method with greatly enhanced electrical conductivity that improved the performance of the inverted planar perovskite solar cells to 17.74%. For solution-processed Cu-doped NiO_x prepared by chemical precipitation method, the only example was given for the inverted-based structure of perovskite solar cells.[32] Thus, up to our knowledge, there exists no reported chemically precipitated Cu-NiO_x HTLs used for both regular and inverted device structures of PSCs.

Herein, we developed a strategy to produce chemically precipitated Cu-NiO_x NPs that form aggregate-free solution in isopropanol (IPA) suitable for processing the HTL on top of photoactive layers. We found out that Cu doping level impacts directly the solubility of Cu-NiO_x NPs in IPA. This allows in optimal conditions to obtain highly soluble NPs solutions stable over several months. The Cu-NiO_x IPA solutions were used to process both regular and inverted-based device structures of PSCs. The initial work function of Cu-NiO_x HTLs was found around 4.5 eV and had to be increased in order to prevent energy loss at the interfaces.[33]

By introducing a strong electron acceptor such as 2,3,5,6-tetrafluoro-7,7,8,8-tetracyanoquinodimethane (F4-TCNQ) into Cu-NiO_x layers, the WF was tuned from 4.47 eV to 5.45 eV, favoring an energy level alignment of Cu-NiO_x with several donor materials having different HOMO energy levels. F4-TCNQ is a well-known p-type dopant used to dope not only interfacial layers but also photoactive layers.[34] The organic-inorganic doped NiO_x nanoparticle composites form highly effective HTLs for regular device structure, leading to PCEs of 7.4% in fullerene solar cells using PTB7:$PC_{70}BM$ blends. Applied to NFA-based solar cells using the polymer donor named poly[(2,6-(4,8-bis(5-(2-ethylhexyl-3-fluoro)thiophen-2-yl)-benzo[1,2-b:4,5-b']dithiophene))-alt-(5,5-(1',3'-di-2-thienyl-5',7'-bis(2-ethylhexyl)benzo[1',2'-c:4',5'c']dithiophene-4,8-dione)] (PBDB-T-2F) and the non-fullerene acceptor named 3,9-bis(2-methylene-((3-(1,1-dicyanomethylene)-6,7-difluoro)-indanone))-5,5,11,11-tetrakis(4hexylphenyl)-dithieno[2,3-d:2',3'-d']-s-indaceno[1,2-b:5,6-b']dithiophene (IT-4F) with inverted device structure, these hybrid HTLs lead to PCE of 7.9% compared to 11% obtained with evaporated MoO_x as well as 6.3% reached with PEDOT:PSS. In both normal and inverted device structures, the losses are induced by optical losses and not by the thickness of the HTL. This demonstrates that the developed solution-processed organic-inorganic Cu-NiO_x NPs are a first step towards efficient HTLs for NFA-based solar cells with inverted device structures without thickness limitation. Additionally, we show for the first time that Cu-NiO_x HTLs can introduce the so-called optical spacer (OSP) effects in inverted device structures that were so far only reported in regular structures using electron transport materials (such as ZnO).[35] These OSPs modify the light distribution inside the devices,[36] allow color tuning and optimize the generated photocurrent of the PBDB-T-2F:IT-4F based polymer solar cells by simply varying the thicknesses of both the photoactive layer and the Cu-NiO_x HTL.

2. Results and discussion

2.1 Synthesis and characterization of nickel oxide nanoparticles

Non-stoichiometric NiO_x NPs were obtained using the chemical precipitation method reported by Jiang *et al.*[18] with some modifications starting with the commercially available nickel nitrate hexahydrate ($Ni(NO_3)_2 \cdot 6H_2O$) and sodium hydroxide (NaOH). These materials were easily dissolved in deionized water. After the dropwise addition of NaOH into the nickel nitrate, the clear green aqueous solution turned turbid. Through accurately controlling the solution pH value to 10, nickel hydroxide $Ni(OH)_2$ was obtained in a considerable yield. The obtained apple green product was washed twice then dried and calcined at 270 °C for 2 hours in air to produce dark-black powder. This calcination procedure was based on the thermal decomposition of $Ni(OH)_2$ to produce non-stoichiometric NiO_x NPs. In fact, the 270 °C is the optimal calcination temperature for NiO_x that allows the presence of small amounts of unreacted nickel hydroxide and nitrate ions critical for stabilizing the dispersion.[28]

The same procedure was followed for synthesizing Cu-doped NiO_x but with the addition of copper nitrate hydrate ($Cu(NO_3)_2.xH_2O$) metal precursor in the starting solution. Cu-NiO_x NPs with copper doping levels ranging from 2% up to 20% were produced by varying the initial molar ratio of the metal precursor with respect to the nickel nitrate while keeping all the other parameters and synthetic steps unchanged. Importantly, and as expected, it was proven that the nominal doping levels corresponding to the initial precursor ratios of the metal dopants to nickel atoms, have resulted in lower doping levels inside the NPs as determined by elemental analysis using an Atomic Absorption Spectroscopy (AAS)**.** The results are summarized in **Table S-1**.

Transmission Electron Microscopy (TEM) analysis was performed to determine the particle size and the crystallinity of the NiO_x NPs. **Figure 1a** and **1b** present the low magnification TEM images of the pristine NiO_x and the Cu-$NiO_{x(12.2\%)}$ NPs, respectively. It was obvious that the crystal size of the doped NiO_x NPs (5 nm) was smaller than that of the pristine NiO_x NPs (10 nm). Meanwhile, both of them show clear lattice fringes, suggesting good crystalline properties of these NPs.

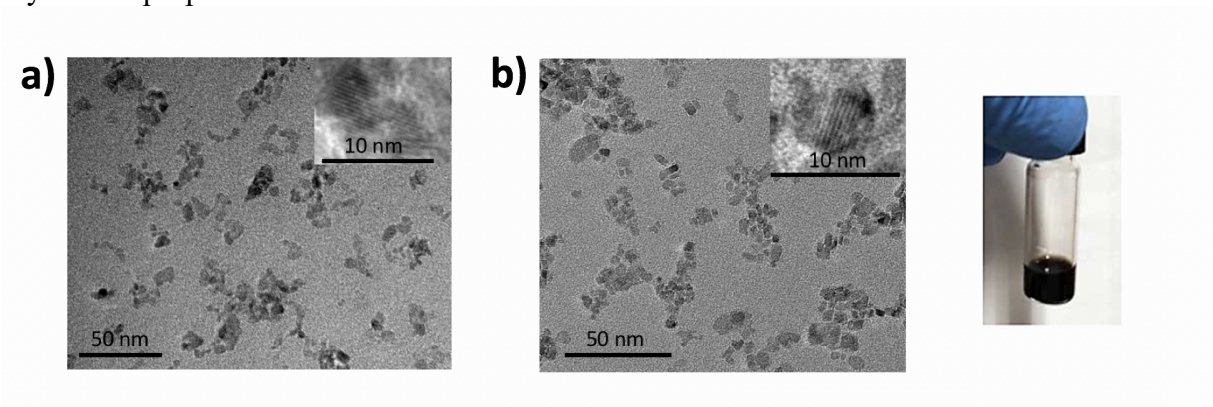

Figure 1. TEM images of non-stochiometric (a) pristine NiO_x and (b) Cu-$NiO_{x(12.2\%)}$ NPs with scale bar of 50 nm.

X-Ray Diffraction (XRD) measurements were performed to explore the crystal structure of both pristine and Cu-doped NiO_x NPs. XRD diffractograms are shown in **Figure 2a**. The diffraction peaks of the pristine NiO_x NPs revealed cubic crystal structure with three prominent characteristic diffraction peaks at 37.29°, 43.34° and 62.91°, which could be assigned to (111), (200) and (220) planes of NiO_x, respectively. Meanwhile, no extra diffraction peaks related to metallic Cu or to copper oxide phase were observed in the XRD diffractogram of Cu-doped NiO_x NPs, indicating that doping with Cu did not hardly change the phase structure of NiO_x. Furthermore, it could be observed that the diffraction peaks were slightly shifted toward lower angles upon increasing the Cu-doping content. This suggests that the lattice parameter of NiO_x was increased upon doping. This was originated from the substitution of Ni ions (ionic radius: 69 pm) with the slightly larger Cu ions (ionic radius: 73 pm).[37] The broadening of the diffraction peaks by increasing the content of Cu ions from 2 to 15% could be related to the presence of smaller crystallites since the incorporation of impurities in oxide semiconductors is known to suppress the grain growth and thus results in smaller particles.[32] These results are in consistence with the TEM results.

Although no crystal phase other than NiO_x was detected using XRD, X-Ray Photoelectron Spectroscopy (XPS) measurements were done to demonstrate the effective doping of the NiO_x NPs with Cu and to investigate the chemical components of the pristine and the doped NiO_x films. The XPS spectra for the pristine NiO_x films are shown in **Figure 2b**. The Ni $2p_{3/2}$ level at 860 eV and the O 1s level at 532.2 eV correspond to the Ni^{3+} state of the NiOOH species. The Ni $2p_{3/2}$ level at 855 eV and the O 1s level at 531 eV peaks can be assigned to the Ni^{3+} state of the Ni_2O_3. In addition, the presence of the Ni^{2+} state of NiO_x is revealed by the Ni $2p_{3/2}$ level at 853.6 and O 1s level at 529 eV peaks as well as the Ni $2p_{1/2}$ peak and its satellites at 873.6 and 878.5 eV. These results are in consistence with the XPS measurements of the previously synthesized NiO_x NPs by Jiang *et al.*[18] The coexistence of Ni^{2+} and Ni^{3+} states is a confirmation of the non-stoichiometric nature of the NiO_x. The XPS spectra of the Cu-$NiO_{x\ (12.2\%)}$ films proved that Cu atoms have been successfully incorporated into the NiO_x

NPs due to the presence of two peaks located at 933.3 and 953.5 eV corresponding to Cu $2p_{3/2}$ and Cu $2p_{1/2}$ levels, respectively. These peaks revealed that Cu^{2+} ions substituted the Ni atom in the NiO_x crystal lattice.[32]

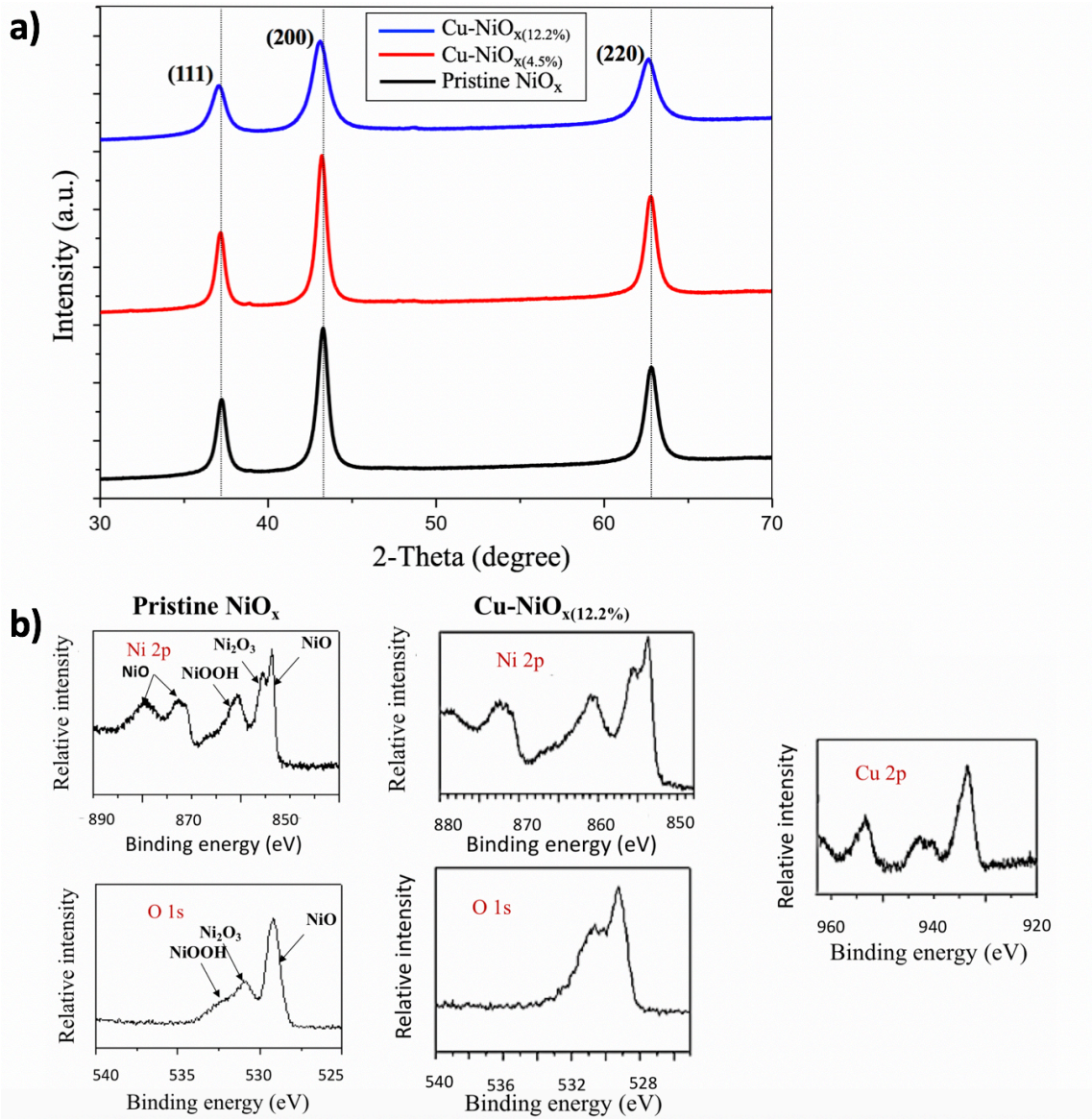

Figure 2. (a) XRD diffractograms and (b) XPS spectra of the pristine and the Cu-$NiO_{x(12.2\%)}$ films showing the Ni 2p, O 1s and Cu 2p core level peaks.

The ultraviolet-visible (UV-vis) absorption spectra of the NiO_x solutions were primarily used to find any possible modification in the energy band structure upon doping. As can be observed in **Figure S-1**, the absorption edge was red-shifted to the visible region upon Cu-doping. This indicates the narrowing of the optical band gap. The band gap of the pristine NiO_x as determined from Tauc plot (3.74 eV) is in good agreement with the reported band gaps.[32] By increasing the Cu-doping level, the band gap was decreased to 3.65, 3.6 and 3.56 eV for Cu-$NiO_{x(2.4\%)}$, Cu-$NiO_{x(12.2\%)}$ and Cu-$NiO_{x(28.2\%)}$, respectively. It was reported that the particle size in the metal oxide systems may affect the electronic properties (such as the band gap) of the NPs due to quantum confinement effect. However, it was also proven that not only quantum confinement can

affect the electronic structure, but also doping can have an impact by introducing defect centers into the lattice. These defects can interact with the host lattice to alter the band structure and cause large changes in their properties.[38] This phenomenon proved again that Cu was successfully included into the NiO_x NPs.

2.2 Solution-processing of NiO_x nanocrystals (NCs)

2.2.1 Alcoholic-based NiO_x solutions

Pristine and the Cu-doped NiO_x nanoparticles with different doping percentage levels can be easily dispersed in water as mentioned elsewhere in literature.[25] It is worth mentioning that the dispersion was dependent on the pH during synthesis. A pH of 10 results in a better dispersion, while any further increase in the basicity of the medium decreases the dispersion of the NPs. This can be related to a previous study showing the effect of pH on the outcome of the precipitation reaction. Nickel salt solutions tend to be acidic (pH ≈ 3) and upon the addition of a strong alkali, precipitation takes place at pH=5.5–6. Thus, it was proven that $Ni(OH)_2$ produced at pH=10-12 is a material deficient in hydroxyl ions and requires the inclusion of nitrates for charge neutrality. However, the NPs produced at higher pH are stoichiometric. Therefore, the increase in the basicity of the medium eliminates the presence of nitrates.[39] On its turn, Jaramillo and coworkers[28] proved the importance of the presence of an amorphous phase containing nitrates, sodium and hydroxides to get a better dispersion of the NiO_x NPs. Thus, not only the calcination temperature but also the pH have an effect on the dispersion of the NiO_x NPs by affecting the final $Ni(OH)_2$ surface product.

It is known that the water-based NiO_x solutions can be easily deposited on top of ITO substrates. However, it is not possible to directly deposit such aqueous solutions on top of photoactive layers in PSCs. As seen in the AFM image of **Figure 3a**, the deposition of Cu-$NiO_{x(12.2\%)}$ solution on top of PTB7:$PC_{70}BM$ photoactive layer resulted in a bad morphology due to the poor wettability of the water-based solutions on the hydrophobic organic blend. This effect is similar to the case of water-based PEDOT:PSS solutions. Normally, wetting agents such as 2,5,8,11-tetramethyl-6-dodecyn-5,8-diolethoxylate (Dynol 604), Zonyl FS300 fluorosurfactant (Zonyl)[40] or Triton-X[41] can be added to the PEDOT:PSS water-based solution to decrease the surface tension, thus improving the wettability on top of photoactive layers. However, such additives showed no effect with the synthesized NiO_x NPs. Therefore, we followed another strategy to transfer the NiO_x dispersion from water into isopropanol by using probe ultrasonication in a mixture of water, isopropanol and methoxy acetic acid surfactant that stabilizes the Cu-NiO_x NPs when transferred into IPA solution. The use of this intermediate step allows producing monodispersed cluster-free IPA-based NiO_x solutions. Dynamic Light Scattering (DLS) measurements shows that the size of the aggregate inside the isopropanol-based solutions corresponds to the size of single NC as determined by TEM.
Additionally, we found that the doping level of the Cu-NiO_x NPs impacts the dispersion of the nanoparticles in IPA. Indeed, the highest solubility and most stable solution in IPA were found for 12.2% of Cu-doping, while pristine NiO_x or NPs with other doping levels showed lower stability. Importantly, the Cu-$NiO_{x(12.2\%)}$ IPA-based solutions were stable for more than six months without occurrence of any NCs aggregation, as confirmed by regular DLS measurements, unlike the aqueous-based solutions having stability not exceeding few days as can be seen in **Figure S-2**.

2.2.2 Thin film processing

Taking into account the importance of the film quality for efficient charge extraction,[42] we studied the morphology of the IPA-based Cu-NiO_x films on ITO substrates as well as on photoactive layers based on PTB7:$PC_{70}BM$ blends by using AFM. As shown in **Figure S-3**, closely-packed layers were observed on ITO with a low surface roughness of 6 nm for the 40 nm-thick Cu-$NiO_{x(12.2\%)}$ layers. Interestingly, the morphology of the Cu-NiO_x layer processed on PTB7:$PC_{70}BM$ is also compact with a 7 nm surface roughness (F**igure 3b**). This indicates that the IPA-based Cu-NiO_x NPs are well adapted for the solution-processing in inverted device structures.

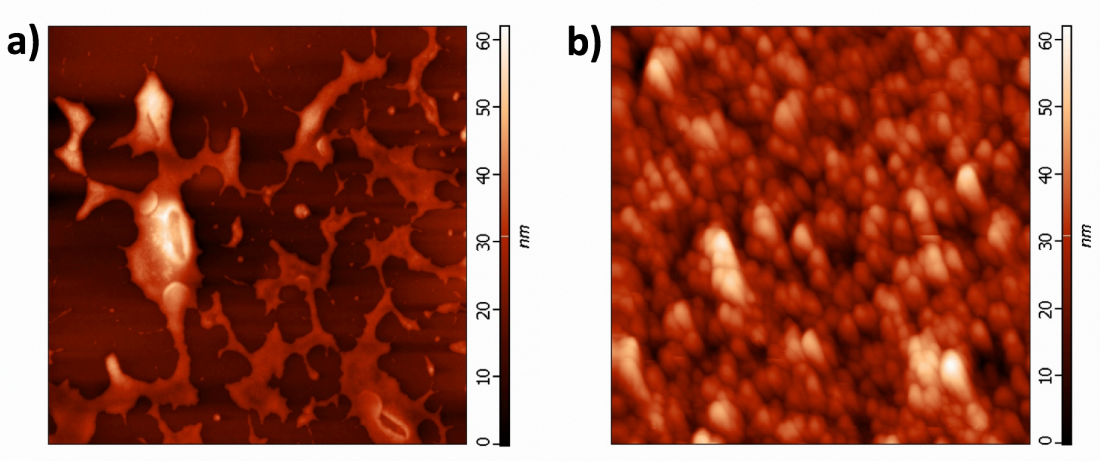

Figure 3. AFM images of (a) water-based Cu-$NiO_{x(12.2\%)}$ and (b) IPA-based Cu-$NiO_{x\ (12.2\%)}$ films deposited on top of PTB7:$PC_{70}BM$ layer.

Transmission spectra of the casted NiO_x films as a function of Cu-doping levels are shown in **Figure S-4**. The 40 nm-thick pristine NiO_x films revealed a high transmission (>80%) in the visible region. As expected, the optical transmittance was slightly decreased with the increase of Cu-doping level. This is attributed to the presence of defect states that are responsible for additional absorption, thus lowering the transmittance as seen before for the doped TiO_2 NPs.[43] Despite this decrease in transmittance, the Cu-$NiO_{x(12.2\%)}$ layers still owe a percentage of transmittance higher than 78% in the visible region. This allows them to function as efficient semi-transparent interfacial layers in polymer solar cells.

2.3 Solar cell devices using Cu-NiO_x HTLs

2.3.1 Regular device structures

In order to evaluate the potential of the Cu-$NiO_{x(12.2\%)}$ as HTLs, PSCs have been first studied in fullerene-based solar cells using a regular device structure with the following architecture: ITO/HTL/PTB7:$PC_{70}BM$/ZnO/Al, as shown in **Figure 4a.** The corresponding solar cells showed poor performance with a PCE of 1.2% when compared to the reference device based on PEDOT:PSS HTL with a PCE of 7.6%. The main losses of the devices using the Cu-$NiO_{x(12.2\%)}$ HTLs were in V_{OC} and FF. It has been shown that different techniques help in suppressing the interface recombination in metal oxide based HTL.[15] In the present case, such losses can be induced by the hole extraction barrier at the interface due to the energy level mismatch between the HOMO of PTB7 and the valence band of Cu-$NiO_{x(12.2\%)}$ HTL. By using

UPS analysis, we found indeed that the Cu-$NiO_{x(12.2\%)}$ layers have a low WF of only 4.47 eV (**Figure S-5**). To improve the electronic properties of the Cu-$NiO_{x(12.2\%)}$ HTLs, we thus applied molecular doping with F4-TCNQ molecule that was found to tune the work function of NiO_x materials.[16] In our work, the molecular doping was performed by spin-coating the F4-TCNQ solution on top of NiO_x HTL.

The UPS measurements of the Cu-$NiO_{x(12.2\%)}$ layers with and without F4-TCNQ are shown in **Figure S-5**. The WF was increased from 4.94 eV to 5.45 eV by increasing the F4-TCNQ concentration from 0.2 to 2 mg mL^{-1}, similarly to NiO_x:F4-TCNQ nanocomposite reported by Cheng *et al.*[16] Consequently, solar cells using a 40 nm-thick Cu-$NiO_{x(12.2\%)}$ with different F4-TCNQ concentrations from 0.2 to 1 mg mL^{-1} were processed in order to study the impact of the WF tuning on the photovoltaic parameters of the devices. The J-V curves of the devices are shown in **Figure 4b** and the photovoltaic parameters are summarized in **Table 1**. An optimal performance was found for 1 mg mL^{-1} F4-TCNQ leading to a PCE of 7.4%, a FF of 60%, a V_{OC} of 751 mV and a J_{SC} of 16.6 mA cm^{-2}. This is comparable to that obtained using PEDOT:PSS HTLs with a PCE of 7.6%. Further increase in the F4-TCNQ concentration causes a drop in V_{OC} and FF. These losses could be related to the high WF (5.45 eV) as well as the potential additional resistances generated by the F4-TCNQ layer. We also studied the impact of the HTL thickness on the device performance. The optimized Cu-$NiO_{x(12.2\%)}$ thickness was found at 40 nm, as thinner layers of 15 nm showed less compact layer morphology, while further increase in the HTL thickness caused a decrease in efficiency mainly due to a drop in J_{SC} (see **Figure S-6**). The later can be related to the increased absorption of the thicker Cu-NiO_x HTLs.

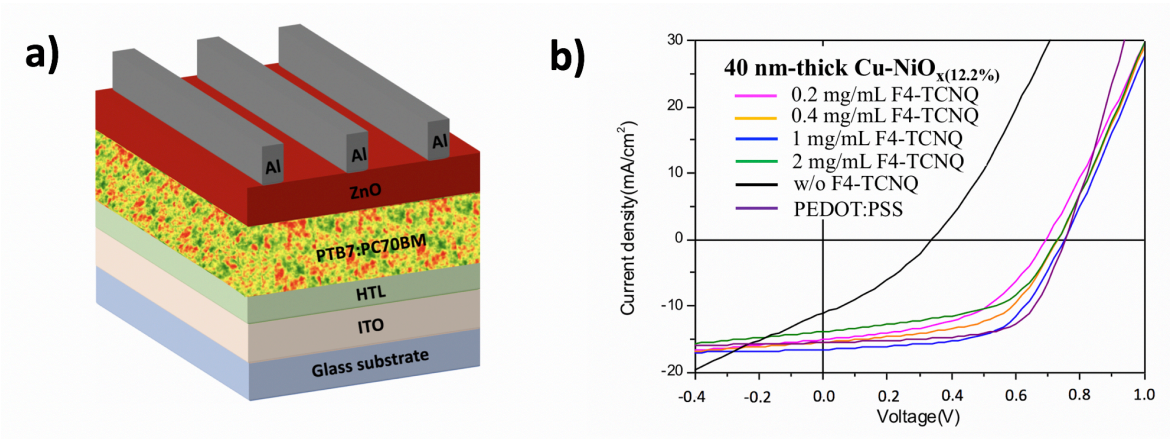

Figure 4. (a) The architecture of the studied regular device structure and (b) typical J-V curves of the PTB7:$PC_{70}BM$-based devices using different HTLs.

[F4-TCNQ] (mg mL^{-1})	V_{OC} (mV)	J_{SC} (mA cm^{-2})	FF (%)	PCE (%)
w/o	340	11.05	33	1.2
0.2	693	15	50	5.2
0.4	730	15.5	55.2	6.2
1	751	16.6	60	7.4
2	729	13.9	53	5.3
PEDOT:PSS	752	15.5	65	7.6

Table 1. Summary of photovoltaic parameters of the PTB7:$PC_{70}BM$ regular-based devices using different HTLs.

2.3.2 Inverted device structures

After optimizing the Cu-$NiO_{x(12.2\%)}$ HTLs in regular device structures, these alcoholic-based Cu-$NiO_{x(12.2\%)}$ HTLs were used for the first time in an inverted device structure as a replacement of the classical evaporated MoO_3. For such a device architecture, the non-fullerene acceptors have attracted strong attention as they possess an improved visible-NIR light-harvesting capability and good electron mobility, thus, delivering higher J_{SC} and PCE in solar cells than fullerene acceptors.[1]

In this regard, we focused our studies on the inverted device structures using PBDB-T-2F:IT-4F photoactive layers. The studied device architecture is ITO/ZnO/80 nm-thick PBDB-T-2F:IT-4F/HTL/Ag as shown in **Figure 5a**. The J-V curves of the corresponding devices are presented in **Figure 5b** and the photovoltaic parameters are summarized in **Table 2.** As a reference cell, an efficiency of 11% was obtained using a 2 nm-thick evaporated MoO_3 with a 62% FF after post-annealing the whole device at 100 °C for 10 minutes. By replacing the evaporated HTL with a 40 nm-thick molecularly doped Cu-$NiO_{x\,(12.2\%)}$, the optimized efficiency obtained was 7.92% with a FF of 53.3%, a V_{OC} of 827 mV and a J_{SC} of 18 mA cm^{-2}. The lower PCE, compared to the reference cells using MoO_x, is due to losses in all photovoltaic parameters indicating that the HTL is not yet fully optimized for the NFA-based solar cells.

The drops in V_{OC} and FF indicate still residual misalignments of the interface levels leading to barriers for hole extraction. For comparison, we also processed devices using modified PEDOT:PSS inks with suitable wettability properties for processing on top of polymer blend. These inks have been previously optimized for fullerene-based blends. As can be seen in **Figure S-7** and **Table 2**, these devices show clearly lower performances compared to the devices processed with the hybrid HTLs. Indeed, even stronger losses in Voc and FF are found for PEDOT:PSS-based devices, indicating the occurrence of strong interfacial losses compared to cells using fullerene acceptors. While the performance losses in Voc and FF need further improvement in the electronic properties of the hybrid HTL, we focus in the following paragraph on the losses in J_{SC} that may be related to optical spacer effects.

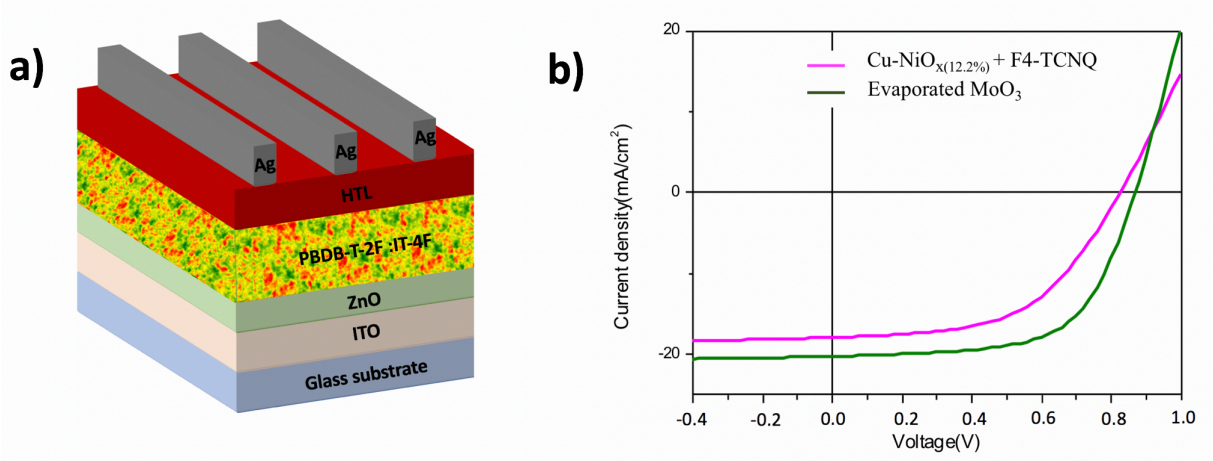

Figure 5. (a) The architecture of the studied inverted device structure and (b) The J-V curves of the PBDB-T-2F:IT-4F-based inverted device structures using different HTLs.

HTL	V_{OC} (mV)	J_{SC} (mA cm^{-2})	FF (%)	PCE (%)
2 nm e-MoO_3	871	20.3	62	11
40 nm Cu-$NiO_{x\ (12.2\%)}$+ F4-TCNQ	827	18	53.3	7.92
40 nm modified PEDOT:PSS	700	19	46.3	6.3

Table 2. Summary of the photovoltaic parameters of the PBDB-T-2F:IT-4F based inverted devices using different HTLs.

2.3.3 Optical spacer effects in inverted device structures

As mentioned previously, by replacing the evaporated MoO_3 with the solution-processed Cu-$NiO_{x(12.2\%)}$ HTL, losses in J_{SC} of around 10% are observed. It is well known that metal oxides such as ZnO can introduce optical spacer effect in polymer solar cells that modifies strongly the light distribution inside the cell and thus the intensity of the photocurrent density.[35,42] While these optical spacer effects have been only described in devices using regular structures, it is possible that the J_{SC} losses in inverted device structures, as used here, may be also related to such effects. In order to study the optical effects more in details, the photonic absorption inside the photoactive layer as function of both the photoactive layer and HTL thickness was investigated using a transfer matrix method.[42] The device structure used for the calculation was ITO/ZnO/PBDB-T-2F:IT-4F/Cu-$NiO_{x(12.2\%)}$+F4-TCNQ/Ag. The polymer blend and the HTL thicknesses were varied from 0 to 300 nm and 0 to 70 nm, respectively, while the thicknesses of the other layers were kept constant (150 nm for the ITO layer, 15 nm for the ZnO layer, and 100 nm for the Ag layer). The optical indices of ITO, ZnO and Ag were taken from literature[42,44] while the optical indices of PBDB-T-2F:IT-4F and Cu-$NiO_{x(12.2\%)}$ layers were determined by spectroscopic ellipsometry (SE) (see the Experimental Section and **Figure S-8**). **Figure 6a** shows the total number of photons absorbed inside the photoactive layer as a function of the photoactive layer thickness for different Cu-$NiO_{x(12.2\%)}$ thicknesses. Two maxima appear in the absorption curve, which are related to interferential phenomena occurring in the thin film stacks.[44,35,45]

The first maximum corresponds to blend thicknesses ranging from 50 to 90 nm with the exact position of each maximum depending on the Cu-NiO_x layer thickness. The second maximum is broader with photoactive layer thicknesses ranging from 170 to 250 nm. These simulations reveal that, for thin photoactive layers, the Cu-NiO_x-based HTLs always lead to a reduction of light absorption inside the active layer compared to solar cells processed without any HTL. In contrast, using thick blend layers, light absorption is almost unchanged as long as the HTL is not surpassing 40-50 nm range. This finding is identical to solar cells using the regular device structures with ZnO or aluminum-doped ZnO as optical spacers.[42,35] Here, the solar cells using Cu-$NiO_{x(12.2\%)}$ HTL have 80 nm-thick photoactive layers that were optimized for the ultrathin MoO_3 HTLs. This is comparable to the situation of the red curve in **Figure 6a**, considering that devices using a 2 nm-thick MoO_3 have almost equivalent absorption to those processed without any HTL. The use of a 40 nm-thick Cu-$NiO_{x(12.2\%)}$ HTL reduced strongly the amount of the absorbed light in the photoactive layer by approximately 10-15%, as shown on the vertical red dotted line as eye guide. By considering these calculations, we indeed find the corresponding losses in J_{SC} for the devices fabricated with Cu-$NiO_{x(12.2\%)}$ (18 mA cm^{-2}) when compared to the reference cells done with MoO_3 generating 20.3 mA cm^{-2}. These calculations allow also to discuss the most suitable conditions for the developed Cu-$NiO_{x(12.2\%)}$:F4-TCNQ bilayers used

in inverted device structures. By considering a 40 nm-thick Cu-$NiO_{x(12.2\%)}$ HTL, the photoactive layer should be at least 180 nm in order to limit the optical losses.

As it was shown recently, the use of optical spacers allows also to modify the color of polymer solar cells.[35] Indeed, the HTLs not only modify the amount of light absorbed inside the active layer but also determine the light reflection of the solar cell, thus affecting the color of the devices. To estimate the potential of the Cu-NiO_x optical spacers in generating colored polymer solar cells, we calculated the color coordinates of the devices in the reflection mode as function of the photoactive layer and Cu-NiO_x thicknesses. Thus, for a 40 nm-thick Cu-$NiO_{x(12.2\%)}$ HTL, the color coordinates corresponding to the reflected light were calculated for photoactive layer thicknesses ranging between 80 and 250 nm. **Figure 6b** is a chromaticity diagram showing a comparison between the calculated and the measured color coordinates of three different solar cells (B, G and P) with different blend thicknesses (80, 180 and 250 nm, respectively). One can first notice that, as expected, the color of the devices can be strongly tuned by adjusting the photoactive layer thickness, thus comparable to solar cells using regular device structure having ZnO electron transport layers. For an 80 nm-thick photoactive layer, the devices have a blue color. They become successively green and pink when the active layer thickness was increased to 180 and 250 nm, respectively. Importantly, very good agreements were found between the color coordinates obtained from simulations with the different measured colors of the three solar cells. Thus, these results show that a large palette of colors can be produced with this technique, making fine-tuning of the color possible *via* adjusting the Cu-NiO_x optical spacer and the photoactive layer thicknesses, thanks to the control in the light absorption amount.

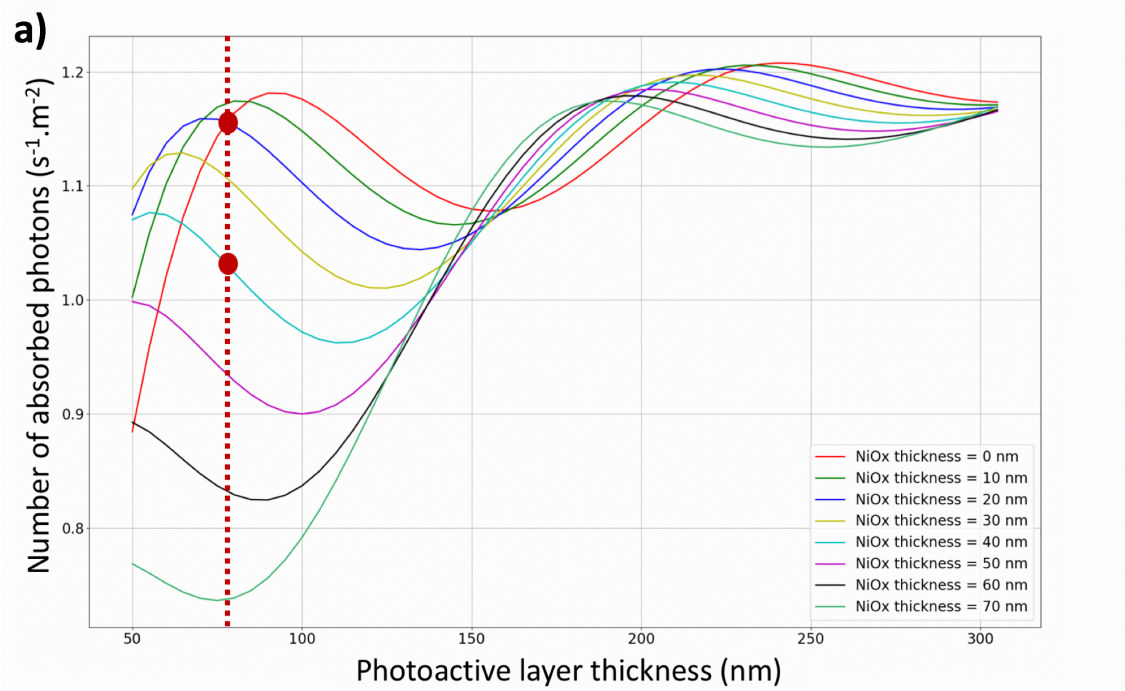

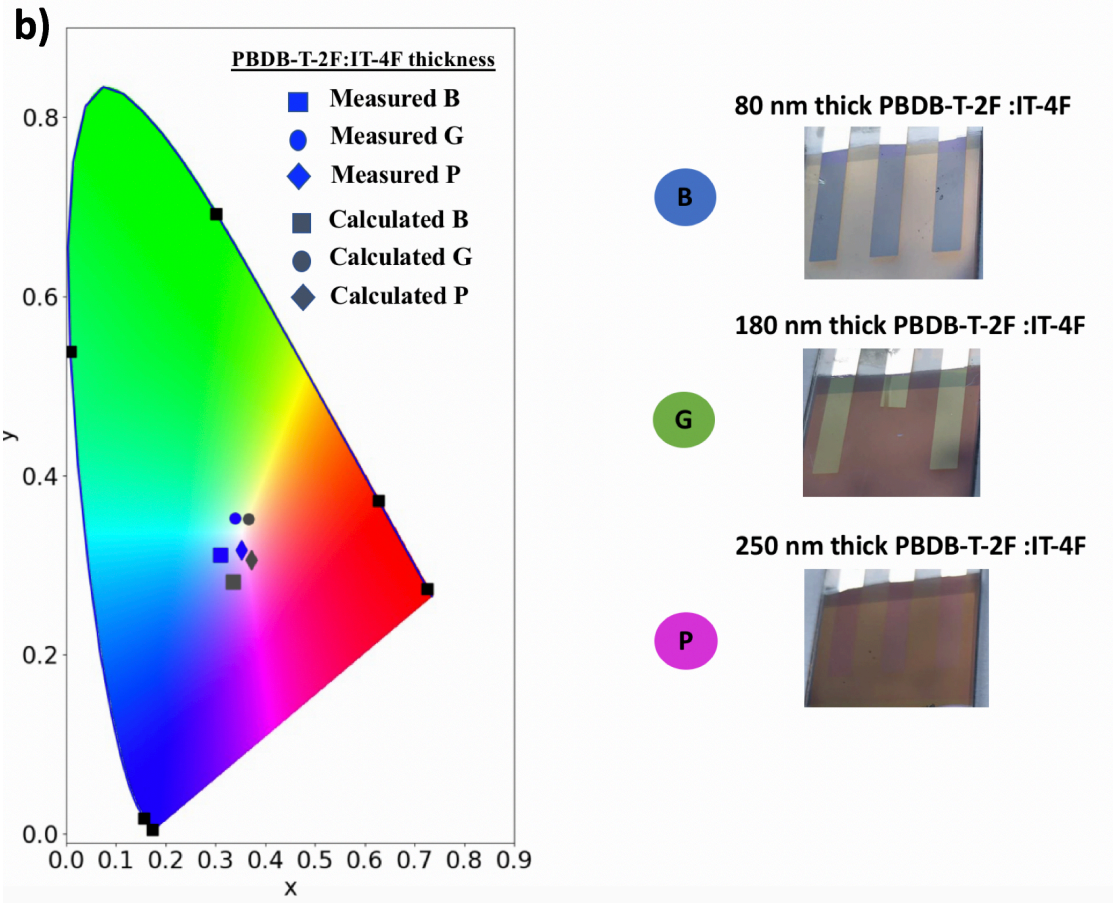

Figure 6. (a) The theoretical total number of photons absorbed inside the PBDB-T-2F:IT-4F photoactive layer as a function of photoactive layer thickness for different Cu-$NiO_{x(12.2\%)}$ thicknesses. (b) Measured (blue dots) and calculated (grey dots) color coordinates for the three experimental Blue, Green and Pink solar cells (left) and photograph images of the corresponding cells (right).

3. Conclusion

Nickel oxide nanoparticles in alcoholic solutions were developed in this work for processing hole transport layers and were applied to non-fullerene acceptor-based solar cells using inverted device structures. We show that copper doping of NiO_x nanoparticles is beneficial to reach aggregate-free solution suitable for processing the HTL on top of photoactive layers. Further doping of these nanoparticles with the organic electron acceptor F4-TCNQ was necessary to optimize the work function of the HTL for efficient hole extraction. Solar cells using normal device structures revealed that such hybrid HTL can be processed up to 45 nm without inducing electric losses due to optimized work function and high conductivity. Processing the hybrid HTLs on top of polymer blends based on IT-4F and PBDB-T-2F led to solar cells with promising efficiencies up to 7.9%, while further work function optimization is needed to reach fully optimized solution-processed organic-inorganic Cu-NiO_x nanoparticles for NFA-based solar cells using inverted device structure. We also demonstrated for the first time that the use of the hybrid HTL in the inverted device structure of polymer solar cells allows for color tuning over a large palette using optical spacer effects. Our future work will focus on the optimization of the work function and transport properties of the organic-inorganic doped NiO_x HTL by combining 2D-materials such as graphene oxide to generate highly efficient HTLs for fully solution-processed solar cells using NFAs with improved air stability.

4. Experimental Section

Synthesis of Highly soluble NiO_x NPs: All the materials were purchased from Sigma Aldrich unless specified elsewhere. NiO_x NPs were prepared by a chemical precipitation method according to a previous report.[18] Typically, 0.05 mole of $Ni(NO_3)_2 \cdot 6H_2O$ were dispersed in 100 mL deionized water. A dark green solution was obtained. Under continuous magnetic stirring, the pH of the solution was adjusted to 10 by the dropwise addition of 10 M NaOH aqueous solution. The pH value was measured by a pH meter (Hanna HI 8417 pH meter). After stirring for 10 minutes, the green colloidal precipitate was washed twice by deionized water using centrifugation and dried at 80 °C overnight. To ensure a complete calcination, the obtained green solid was ground to finer powder using a pestle and a mortar, then calcined at 270 °C for 2 hours to yield a black powder. For the Cu-NiO_x NPs, the same procedure was followed. The only difference is the addition of the $Cu(NO_3)_2 \cdot xH_2O$ precursor in the initial solution at various molar ratios (from 2 to 20%).

Preparation of the NiO_x solutions: NiO_x NPs were dispersed in water to the desired concentration. Then, the solution was transferred to IPA solvent and dispersed using a probe ultrasonication until obtaining an aggregate-free solution.

Preparation of the ZnO solutions: ZnO NPs were prepared as published elsewhere.[46,47] The cluster-free ZnO nanoparticle solution of 5 mg mL^{-1} was prepared by transferring the as-synthesized ZnO nanoparticles from methanol into isopropanol mixed with ethanolamine (0.2 vol.%).

Characterization Methods: The NiO_x NCs were characterized by HR-TEM (JEOL 3010, acceleration voltage of 300 kV). The samples were prepared by drop-casting a diluted isopropanol solution of NiO_x NCs onto a carbon-coated copper grid. UV–vis absorption of the NiO_x NCs in solution and on films were recorded using a Varian CARY 50 spectrophotometer.

Size distribution of the NCs within the solution was determined by DLS using a NanoZetaSizer from Malvern. Crystallinity of the NiO_x NCs was measured by XRD using an INEL with a linear detector. AFM was realized using a NTEGRA Prima of the brand NT-MDT in taping mode to study the quality of the NiO_x NCs layers. Layer thicknesses were determined using a mechanical profilometer. Photoemission spectroscopy using UV (UPS, HeI 21.2 eV) and X-ray (XPS, monochromatized Al Kα 1486.7 eV) light sources were performed at Linkoping University in Sweden.

Optical Simulations of the Solar Cells: Ellipsometry has been used to extract the optical indices of Cu-NiO_x thin films. The measurements have been performed for wavelengths ranging between 380 and 1000 nm using a Semilab rotating compensator ellipsometer equipped with a microspot which focuses the beam on a very small area of the sample (a circle with a diameter of 100 μm).

The layers were coated on glass substrates. SEA software (Semilab company) was used to fit the SE measurements of tan (Ψ) and cos (Δ) and extract the optical indices $n(\lambda)$ and $k(\lambda)$ of the materials. The dielectric functions $\varepsilon = \varepsilon_1 + i*\varepsilon_2$ of PBDB-T-2F:IT-4F have been fitted with Gaussian model that is adequate for the parameterization of the optical functions of amorphous thin films in the interband region.[48] The dielectric functions of Cu-$NiO_{x(12.2\%)}$ have been fitted with a Gauss-Sellmeyer model in order to take into account both the dielectric and the absorbing character of this material. The optical indices of PBDB-T-2F:IT-4F and Cu-$NiO_{x(12.2\%)}$ are shown in **Figure S-8**. While the optical indices of ITO, ZnO and Ag were taken from literature.[42,44] The CIE xyY (1931) model has been employed for the color prediction of the polymer solar cells. This model allows calculating the normalized color coordinates (x, y) of solar cells from their reflection spectra by considering the human eye sensitivity. Using the optical indices of the materials as input parameters, the reflection spectra of the solar cells have been calculated using a transfer matrix method.[45] The reflection spectra of the cells were carried out using a Perkin Elmer spectrophotometer Lambda 950.

Solar Cell Fabrication: The organic-BHJ solar cells were prepared following several steps. First, the ITO substrates (15 Ω sq^{-1}) were cleaned by deionized water, acetone, ethanol, and isopropanol with ultrasonication. Then, the pre-cleaned ITO substrates were exposed to UV-ozone treatment for 15 min to reform the surface. In the case of regular device structures, a thin layer of PEDOT:PSS (Heraeus, CLEVIOS PVP AI 4083) was spin-coated on the pre-cleaned ITO substrates at a speed of 3500 rpm for 60 s followed by heating on a hotplate at 140 °C for 20 min to obtain a film thickness of ≈40 nm. The NiO_x HTLs were spin-coated at 2500 rpm for 60 s from different concentrations (10 to 30 mg mL^{-1}) to obtain different film thicknesses. These NiO_x films were then annealed on a hot plate in air at 80 °C for 10 min. A solution of F4-TCNQ (Ossilla) with different concentrations (from 0.2 to 2 mg mL^{-1}) was spin-coated with the same speed and annealed at 80 °C for 30 min. The substrates were then transferred into a nitrogen-filled glovebox. The PTB7:$PC_{70}BM$ blend solution was prepared from the weight ratio of 1:1.5 and a total concentration of 25 mg mL^{-1} in chlorobenzene with 0.3 vol% 1,8-diiodooctane processing additive. After stirring overnight at 60 °C, the BHJ thin films (90 nm) were obtained from spin-coating the solution at 1800 rpm for 120 s. The active layers were then transferred into high vacuum for overnight. ZnO NCs were processed by spin-coating a 5 mg mL^{-1} solution on top of the active layers at 1500 rpm for 60 s followed by annealing for 2 min at 80 °C. The top Al metal electrode (100 nm) was thermally evaporated at 1×10^{-6} Torr pressure through a shadow mask with a device area of 0.27 cm^2.

For the inverted device structures, 1 wt.% ZnO (Avantama) was spin-coated on top of the pre-cleaned ITO substrates at 5000 rpm for 60 s then annealed at 120 °C for 10 min in air. The PBDB-T-2F:IT-4F solution was prepared from a weight ratio 1:1 and a total concentration of 20 mg mL^{-1} in o-xylene. After stirring overnight at room temperature, the active layers were prepared by spin-casting the ink at 2200 rpm for 2 min (without annealing). A 2 nm-thick MoO_3 layer and a 100 nm-thick silver layer were then thermally evaporated onto the surface of the active layer at 2×10^{-6} Torr pressure through a shadow mask. For each device configuration, a total of six cells were measured. The current density-voltage (J-V) characteristics of the devices were measured using a Keithley 238 Source Measure Unit. Solar cell performance was measured using a Newport classe AAA 1.5 Global solar simulator (Oriel Sol3ATM model n° 94043A) with an irradiation intensity of 100 mW cm^{-2}. The light intensity was determined with a Si reference cell (Newport Company, Oriel n° 94043A) calibrated by National Renewable Energy Laboratory (NREL).

Conflicts of interest

There are no conflicts to declare.

Acknowledgments

The authors thank Alain Ranguis, Damien Chaudanson and Vasile Heresanu from CINaM laboratory for their assistance in the use of AFM, TEM and XRD facilities. They also acknowledge Igor Ozerov and Frédéric Bedu for the profilometer measurements performed at the PLANETE CT PACA cleanroom facility.

References

1 Q. Liu, Y. Jiang, K. Jin, J. Qin, J. Xu, W. Li, J. Xiong, J. Liu, Z. Xiao, K. Sun, S. Yang, X. Zhang and L. Ding, 18% Efficiency organic solar cells, *Sci. Bull.*, 2020, **65**, 272–275.

2 R. Po, C. Carbonera, A. Bernardi and N. Camaioni, The role of buffer layers in polymer solar cells, *Energy Environ. Sci.*, 2011, **4**, 285–310.

3 A. N. Bartynski, C. Trinh, A. Panda, K. Bergemann, B. E. Lassiter, J. D. Zimmerman, S. R. Forrest and M. E. Thompson, A Fullerene-Based Organic Exciton Blocking Layer with High Electron Conductivity, *Nano Lett.*, 2013, **13**, 3315–3320.

4 M. C. Scharber, D. Mühlbacher, M. Koppe, P. Denk, C. Waldauf, A. J. Heeger and C. J. Brabec, Design Rules for Donors in Bulk-Heterojunction Solar Cells—Towards 10 % Energy-Conversion Efficiency, *Adv. Mater.*, 2006, **18**, 789–794.

5 Y. Xia, K. Sun and J. Ouyang, Solution-Processed Metallic Conducting Polymer Films as Transparent Electrode of Optoelectronic Devices, *Adv. Mater.*, 2012, **24**, 2436–2440.

6 Q. Li, J. Yang, S. Chen, J. Zou, W. Xie and X. Zeng, Highly Conductive PEDOT:PSS Transparent Hole Transporting Layer with Solvent Treatment for High Performance Silicon/Organic Hybrid Solar Cells, *Nanoscale Res. Lett.*, 2017, **12**, 506.

7 Y. Meng, Z. Hu, N. Ai, Z. Jiang, J. Wang, J. Peng and Y. Cao, Improving the Stability of Bulk Heterojunction Solar Cells by Incorporating pH-Neutral PEDOT:PSS as the Hole Transport Layer, *ACS Appl. Mater. Interfaces*, 2014, **6**, 5122–5129.

8 W.-H. Baek, M. Choi, T.-S. Yoon, H. H. Lee and Y.-S. Kim, Use of fluorine-doped tin oxide instead of indium tin oxide in highly efficient air-fabricated inverted polymer solar cells, *Appl. Phys. Lett.*, 2010, **96**, 133506.
9 Y.-J. Cheng, C.-H. Hsieh, Y. He, C.-S. Hsu and Y. Li, Combination of Indene-C60 Bis-Adduct and Cross-Linked Fullerene Interlayer Leading to Highly Efficient Inverted Polymer Solar Cells, *J. Am. Chem. Soc.*, 2010, **132**, 17381–17383.
10 S. K. Hau, H.-L. Yip, H. Ma and A. K.-Y. Jen, High performance ambient processed inverted polymer solar cells through interfacial modification with a fullerene self-assembled monolayer, *Appl. Phys. Lett.*, 2008, **93**, 233304.
11 F. Wang, Z. Tan and Y. Li, Solution-processable metal oxides/chelates as electrode buffer layers for efficient and stable polymer solar cells, *Energy Environ. Sci.*, 2015, **8**, 1059–1091.
12 D. Ouyang, Z. Huang and W. C. H. Choy, Solution-Processed Metal Oxide Nanocrystals as Carrier Transport Layers in Organic and Perovskite Solar Cells, *Adv. Funct. Mater.*, 2019, **29**, 1804660.
13 D. Ouyang, J. Xiao, F. Ye, Z. Huang, H. Zhang, L. Zhu, J. Cheng and W. C. H. Choy, Strategic Synthesis of Ultrasmall $NiCo_2O_4$ NPs as Hole Transport Layer for Highly Efficient Perovskite Solar Cells, *Adv. Energy Mater.*, 2018, **8**, 1702722.
14 B. Yang, D. Ouyang, Z. Huang, X. Ren, H. Zhang and W. C. H. Choy, Multifunctional Synthesis Approach of In:$CuCrO_2$ Nanoparticles for Hole Transport Layer in High-Performance Perovskite Solar Cells, *Adv. Funct. Mater.*, 2019, **29**, 1902600.
15 Z. Huang, D. Ouyang, R. Ma, W. Wu, V. A. L. Roy and W. C. H. Choy, A General Method: Designing a Hypocrystalline Hydroxide Intermediate to Achieve Ultrasmall and Well-Dispersed Ternary Metal Oxide for Efficient Photovoltaic Devices, *Adv. Funct. Mater.*, 2019, **29**, 1904684.
16 J. Cheng, X. Ren, H. L. Zhu, J. Mao, C. Liang, J. Zhuang, V. A. L. Roy and W. C. H. Choy, Pre- and post-treatments free nanocomposite based hole transport layer for high performance organic solar cells with considerably enhanced reproducibility, *Nano Energy*, 2017, **34**, 76–85.
17 Z. Huang, G. Natu, Z. Ji, M. He, M. Yu and Y. Wu, Probing the Low Fill Factor of NiO p-Type Dye-Sensitized Solar Cells, *J. Phys. Chem. C*, 2012, **116**, 26239–26246.
18 F. Jiang, W. C. H. Choy, X. Li, D. Zhang and J. Cheng, Post-treatment-Free Solution-Processed Non-stoichiometric NiO(x) Nanoparticles for Efficient Hole-Transport Layers of Organic Optoelectronic Devices, *Adv. Mater. Deerfield Beach Fla*, 2015, **27**, 2930–2937.
19 M. D. Irwin, D. B. Buchholz, A. W. Hains, R. P. H. Chang and T. J. Marks, p-Type semiconducting nickel oxide as an efficiency-enhancing anode interfacial layer in polymer bulk-heterojunction solar cells, *Proc. Natl. Acad. Sci. U. S. A.*, 2008, **105**, 2783–2787.
20 S.-Y. Park, H.-R. Kim, Y.-J. Kang, D.-H. Kim and J.-W. Kang, Organic solar cells employing magnetron sputtered p-type nickel oxide thin film as the anode buffer layer, *Sol. Energy Mater. Sol. Cells*, 2010, **94**, 2332–2336.
21 Z. Yi Wang, S.-H. Lee, D.-H. Kim, J.-H. Kim and J.-G. Park, Effect of NiOx thin layer fabricated by oxygen-plasma treatment on polymer photovoltaic cell, *Sol. Energy Mater. Sol. Cells*, 2010, **94**, 1591–1596.
22 S. Seo, I. J. Park, M. Kim, S. Lee, C. Bae, H. S. Jung, N.-G. Park, J. Y. Kim and H. Shin, An ultra-thin, un-doped NiO hole transporting layer of highly efficient (16.4%) organic–inorganic hybrid perovskite solar cells, *Nanoscale*, 2016, **8**, 11403–11412.
23 A. Garcia, G. C. Welch, E. L. Ratcliff, D. S. Ginley, G. C. Bazan and D. C. Olson, Improvement of Interfacial Contacts for New Small-Molecule Bulk-Heterojunction Organic Photovoltaics, *Adv. Mater.*, 2012, **24**, 5368–5373.
24 S. Yoon and D.-W. Kang, Solution-processed nickel oxide hole transport layer for highly efficient perovskite-based photovoltaics, *Ceram. Int.*, 2018, **44**, 9347–9352.
25 K. Zilberberg, J. Meyer and T. Riedl, Solution processed metal-oxides for organic electronic devices, *J. Mater. Chem. C*, 2013, **1**, 4796–4815.

26 H. Zhang, J. Cheng, D. Li, F. Lin, J. Mao, C. Liang, A. K.-Y. Jen, M. Grätzel and W. C. H. Choy, Toward All Room-Temperature, Solution-Processed, High-Performance Planar Perovskite Solar Cells: A New Scheme of Pyridine-Promoted Perovskite Formation, *Adv. Mater.*, 2017, **29**, 1604695.
27 X. Yin, P. Chen, M. Que, Y. Xing, W. Que, C. Niu and J. Shao, Highly Efficient Flexible Perovskite Solar Cells Using Solution-Derived NiOx Hole Contacts, *ACS Nano*, 2016, **10**, 3630–3636.
28 J. Ciro, D. Ramírez, M. A. Mejía Escobar, J. F. Montoya, S. Mesa, R. Betancur and F. Jaramillo, Self-Functionalization Behind a Solution-Processed NiOx Film Used As Hole Transporting Layer for Efficient Perovskite Solar Cells, *ACS Appl. Mater. Interfaces*, 2017, **9**, 12348–12354.
29 H. Zhang, J. Cheng, F. Lin, H. He, J. Mao, K. S. Wong, A. K.-Y. Jen and W. C. H. Choy, Pinhole-Free and Surface-Nanostructured NiOx Film by Room-Temperature Solution Process for High-Performance Flexible Perovskite Solar Cells with Good Stability and Reproducibility, *ACS Nano*, 2016, **10**, 1503–1511.
30 J. Cheng, H. Zhang, Y. Zhao, J. Mao, C. Li, S. Zhang, K. S. Wong, J. Hou and W. C. H. Choy, Self-Assembled Quasi-3D Nanocomposite: A Novel p-Type Hole Transport Layer for High Performance Inverted Organic Solar Cells, *Adv. Funct. Mater.*, 2018, **28**, 1706403.
31 J. W. Jung, C.-C. Chueh and A. K.-Y. Jen, A Low-Temperature, Solution-Processable, Cu-Doped Nickel Oxide Hole-Transporting Layer via the Combustion Method for High-Performance Thin-Film Perovskite Solar Cells, *Adv. Mater.*, 2015, **27**, 7874–7880.
32 Q. He, K. Yao, X. Wang, X. Xia, S. Leng and F. Li, Room-Temperature and Solution-Processable Cu-Doped Nickel Oxide Nanoparticles for Efficient Hole-Transport Layers of Flexible Large-Area Perovskite Solar Cells, *ACS Appl. Mater. Interfaces*, 2017, **9**, 41887–41897.
33 J.-Y. Jeng, M.-W. Lin, Y.-J. Hsu, T.-C. Wen and T.-F. Guo, The Roles of Poly(Ethylene Oxide) Electrode Buffers in Efficient Polymer Photovoltaics, *Adv. Energy Mater.*, 2011, **1**, 1192–1198.
34 F. Guillain, J. Endres, L. Bourgeois, A. Kahn, L. Vignau and G. Wantz, Solution-Processed p-Dopant as Interlayer in Polymer Solar Cells, *ACS Appl. Mater. Interfaces*, 2016, **8**, 9262–9267.
35 M. Gaceur, S. B. Dkhil, D. Duché, F. Bencheikh, J.-J. Simon, L. Escoubas, M. Mansour, A. Guerrero, G. Garcia-Belmonte, X. Liu, M. Fahlman, W. Dachraoui, A. K. Diallo, C. Videlot-Ackermann, O. Margeat and J. Ackermann, Ligand-Free Synthesis of Aluminum-Doped Zinc Oxide Nanocrystals and their Use as Optical Spacers in Color-Tuned Highly Efficient Organic Solar Cells, *Adv. Funct. Mater.*, 2016, **26**, 243–253.
36 A. K. K. Kyaw, D. H. Wang, D. Wynands, J. Zhang, T.-Q. Nguyen, G. C. Bazan and A. J. Heeger, Improved Light Harvesting and Improved Efficiency by Insertion of an Optical Spacer (ZnO) in Solution-Processed Small-Molecule Solar Cells, *Nano Lett.*, 2013, **13**, 3796–3801.
37 R. D. Shannon, Revised effective ionic radii and systematic studies of interatomic distances in halides and chalcogenides, *Acta Crystallogr. A*, 1976, **32**, 751–767.
38 M. Singh, M. Goyal and K. Devlal, Size and shape effects on the band gap of semiconductor compound nanomaterials, *J. Taibah Univ. Sci.*, 2018, **12**, 470–475.
39 T. N. Ramesh and P. V. Kamath, Synthesis of nickel hydroxide: Effect of precipitation conditions on phase selectivity and structural disorder, *J. Power Sources*, 2006, **156**, 655–661.
40 A. Savva, M. Neophytou, C. Koutsides, K. Kalli and S. A. Choulis, Synergistic effects of buffer layer processing additives for enhanced hole carrier selectivity in inverted Organic Photovoltaics, *Org. Electron.*, 2013, **14**, 3123–3130.
41 M. Wagner, C. D. O'Connell, D. G. Harman, R. Sullivan, A. Ivaska, M. J. Higgins and G. G. Wallace, Synthesis and optimization of PEDOT:PSS based ink for printing nanoarrays using Dip-Pen Nanolithography, *Synth. Met.*, 2013, **181**, 64–71.
42 S. B. Dkhil, D. Duché, M. Gaceur, A. K. Thakur, F. B. Aboura, L. Escoubas, J.-J. Simon, A. Guerrero, J. Bisquert, G. Garcia-Belmonte, Q. Bao, M. Fahlman, C. Videlot-Ackermann, O. Margeat and J. Ackermann, Interplay of Optical, Morphological, and Electronic Effects of ZnO Optical Spacers in Highly Efficient Polymer Solar Cells, *Adv. Energy Mater.*, 2014, **4**, 1400805.

43 V. R. Akshay, B. Arun, G. Mandal and M. Vasundhara, Visible range optical absorption, Urbach energy estimation and paramagnetic response in Cr-doped TiO2 nanocrystals derived by a sol–gel method, *Phys. Chem. Chem. Phys.*, 2019, **21**, 12991–13004.
44 D. Duché, E. Drouard, JJ. Simon, L. Escoubas, Ph. Torchio, J. Le Rouzo and S. Vedraine, Light harvesting in organic solar cells, *Sol. Energy Mater. Sol. Cells*, 2011, **95**, S18–S25.
45 D. Duché, F. Bencheikh, S. B. Dkhil, M. Gaceur, N. Berton, O. Margeat, J. Ackermann, J. J. Simon and L. Escoubas, Optical performance and color investigations of hybrid solar cells based on P3HT:ZnO, PCPDTBT:ZnO, PTB7:ZnO and DTS(PTTh2)2:ZnO, *Sol. Energy Mater. Sol. Cells*, 2014, **126**, 197–204.
46 G. E. Jellison and F. A. Modine, Parameterization of the optical functions of amorphous materials in the interband region, *Appl. Phys. Lett.*, 1998, **APLCLASS2019**, 371–373.
47 G. Mattioli, S. B. Dkhil, M. I. Saba, G. Malloci, C. Melis, P. Alippi, F. Filippone, P. Giannozzi, A. K. Thakur, M. Gaceur, O. Margeat, A. K. Diallo, C. Videlot-Ackermann, J. Ackermann, A. A. Bonapasta and A. Mattoni, Interfacial Engineering of P3HT/ZnO Hybrid Solar Cells Using Phthalocyanines: A Joint Theoretical and Experimental Investigation, *Adv. Energy Mater.*, 2014, **4**, 1301694.
48 F. Bencheikh, D. Duché, C. M. Ruiz, J.-J. Simon and L. Escoubas, Study of Optical Properties and Molecular Aggregation of Conjugated Low Band Gap Copolymers: PTB7 and PTB7-Th, *J. Phys. Chem. C*, 2015, **119**, 24643–24648.